Earth and Planetary Science Letters 308 (2011) 11–22

Contents lists available at ScienceDirect

Earth and Planetary Science Letters

journal homepage: www.elsevier.com/locate/epsl

Dynamic plumbing system beneath volcanoes revealed by kinetic modeling, and the connection to monitoring data: An example from Mt. Etna

Maren Kahl [a,*], Sumit Chakraborty [a], Fidel Costa [b], Massimo Pompilio [c]

[a] Institut für Geologie, Mineralogie & Geophysik, Ruhr-Universität, Bochum, Bochum 44780, Germany
[b] Earth Observatory of Singapore, Nanyang Technological University, Singapore 639798, Singapore
[c] Istituto Nazionale di Geofisica e Vulcanologia, Sezione di Pisa, Pisa 56126, Italy

ARTICLE INFO

Article history:
Received 17 October 2010
Received in revised form 31 March 2011
Accepted 4 May 2011
Available online 17 June 2011

Editor: L. Stixrude

Keywords:
Mt. Etna
plumbing system
olivine
zoning
timescales
monitoring

ABSTRACT

Our ability to monitor volcanoes (using seismic signals, ground deformation, gas fluxes, or other ground and satellite based observations) as well as our understanding of melt reservoirs that feed eruptions have evolved tremendously in recent years. The complex plumbing systems that are thought to feed eruptions are, however, difficult to relate to the monitoring signals. Here we show that the record preserved in compositional zoning of erupted minerals may be used to reconstruct sections of the plumbing system. Kinetic modeling of such zoning can yield information on the residence time of magma in different segments of the plumbing systems. This allows a more nuanced evaluation of the link between observed monitoring signals or eruption styles and the magmatic processes and movement of batches of melts at depth. The approach is illustrated through a study of the compositional zoning recorded in olivine crystals from the 1991–1993 SE-flank eruption products of Mt. Etna (Sicily). The zoning patterns in crystals reveal that the plumbing system of the volcano consisted of at least three different magmatic environments between which magma was transported and mixed in the year or two preceding the start of eruption. Quantification of this history indicates that two main pathways of melt migration and three timescales dominated the dynamics of the system. Combination of this information with the timing of observation of various monitoring signals allows a reconstruction of the dynamic evolution of this section of the plumbing system during the early stages of the 1991–1993 eruption. It is seen, for example, how the migration of melt through the same sections of the plumbing system can cause pre-eruptive triggering, enhance Strombolian activity, and through the ensuing eruption cleanse and flush the plumbing system. Different kinds of mixing occur simultaneously at different sections of the plumbing system on different timescales (a few days up to two years).

1. Introduction

Our understanding of volcanic processes has increased tremendously in the last couple of decades due to improvements in geophysical and geochemical tools, and through the comprehensive installation of real time monitoring networks (microgravity changes, high resolution seismic and radar observations; e.g. Scarpa and Tilling, 1996). The ability to map changes of a volcanic edifice before, during, and after an eruption has also altered the classical view of magma storage in a simple, single 'magma chamber'. A dynamic plumbing system of interconnected melt reservoirs that define an extended molten region or 'magma mush zone' (e.g., Marsh, 2006) is probably more realistic, particularly in very active volcanic systems. This poses a new challenge for relating the various monitoring signals to movement of melt through a complex network.

Compositional zoning in magmatic crystals may record a series of processes that occur as magma progresses through such complex crystal-melt networks. The use of compositionally zoned minerals, including plagioclase (Ginibre et al., 2002; Milch, 1905; Pearce and Kolisnik, 1990; Vance, 1962, 1965), olivine (Clark et al., 1986; Kohn et al., 1989) and clinopyroxene (Clark et al., 1986; Downes, 1974; Streck et al., 2002) to unravel the sequence of events that occurred in a magmatic system is well established (Anderson, 1984; Ginibre et al., 2007; Helz, 1987; Hibbard, 1981; Humphreys et al., 2006; Singer et al., 1995; Streck, 2008; Wallace & Bergantz, 2002, 2004, 2005). Moreover, kinetic modeling of the diffusive modification of such zonings provides information on the timescale of melt transfer through the plumbing system. Diffusion modeling has been increasingly used to obtain timescales of individual magmatic processes (e.g. Costa et al., 2003; Costa et al., 2008, 2010; Morgan et al., 2004; Morgan and Blake, 2006; Nakamura, 1995; Zellmer et al., 1999).

* Corresponding author. Tel.: +49 234 322 4393; fax: +49 234 321 4433.
E-mail addresses: Maren.Kahl@rub.de (M. Kahl), Sumit.Chakraborty@rub.de (S. Chakraborty), fcosta@ntu.edu.sg (F. Costa), pompilio@pi.ingv.it (M. Pompilio).

0012-821X/$ – see front matter © 2011 Elsevier B.V. All rights reserved.
doi:10.1016/j.epsl.2011.05.008

Here we show that the record preserved in compositionally zoned crystals can be used to map the history of passage of melts through complex plumbing networks, and that kinetic modeling of such zoning provides information on the timescale of such melt movement. The geophysical and geochemical monitoring tools applied to active volcanoes provide us a variety of information that needs to be interpreted as magma movement and/or interaction of magma with surrounding host rocks. However, it is difficult to uniquely relate these monitoring data to specific magma batches or magmatic processes occurring at depth. On the other hand, it is the chemistry of magmas (melts and crystals) that record the intensive thermodynamic variables (e.g. pressure, temperature, volatile content and composition) and the processes relevant for the evolution of a magmatic system. It is a highly desirable goal to be able to relate the time series information from various monitoring tools to specific variations of thermodynamic parameters and magmatic processes, and this manuscript aims at taking an important step toward achieving this goal.

We illustrate the approach using olivine compositions from the eruptive products of the 1991–1993 SE-flank eruption of Mt. Etna (Sicily), one of the best-monitored volcanoes on Earth. Numerous changes in geophysical (e.g. ground deformation, seismicity, microgravity), and geochemical (CO_2 and SO_2 gas emissions) signals were recorded prior to, during, and after this eruption. Olivine was chosen because of its diverse but systematic zoning patterns, and because diffusion coefficients of multiple elements are well known in this mineral. We have inferred a possible plumbing system, and a chronology of magmatic events preceding the eruption that can be related to specific surface monitoring signals. Extension of our observations to interpret the monitoring signals being observed during the current eruptive period (Bonforte et al., 2008) at Mt. Etna or at other well monitored volcanoes should enable us to obtain more realistic inversions of these data and better predict the course of future eruptions.

2. Sequence of events leading to and during the 1991–1993 eruption

The volcanic edifice of Mt. Etna towers about 3330 m a.s.l. on the eastern coast of Sicily and covers a basal area of ~1250 km^2 (Fig. 1). The 1991–1993 SE-flank eruption was preceded by a minor flank eruption in (September–October) 1989 and a series of paroxysmal episodes in early 1990 (Table 1). The flank activity resumed at Mt. Etna in the early hours of December 14, 1991 after a brief repose and was accompanied by a major seismic swarm (~250 events; Patanè et al., 1994). This event occurred after 23 months of quiet summit activity (Falsaperla et al., 1994). A new fracture system with two branches developed and propagated NE and SSE from the base of the Southeast crater (Fig. 1). The NE-branch was mainly characterized by ash and bomb fall and lasted a couple of hours. The SSE-branch propagated downslope to an elevation of 2700 m almost parallel to the 1989 fracture zone (Barberi et al., 1993; Calvari et al., 1994). During the night of 14th of December the eruptive activity continued from the western wall of the Valle del Bove (VdB) (Fig. 1) from eruptive vents between 2400 and 2200 m a.s.l. (Barberi et al., 1993; Calvari et al., 1994; Stevens et al., 1997). Finally, these vents became the source for a persistent effusive activity for the following 473 days. In March 1993 the activity ceased after producing a compound lava flow field of $240 \pm 29 \times 10^6$ m^3 (Calvari et al., 1994; Stevens et al., 1997). The samples studied are from three temporally separated trachybasaltic lava flows that erupted between December 1991 and March 1992 (hereafter the samples are referred as: 14-December-1991, 03-January-1992 and 14-March-1992).

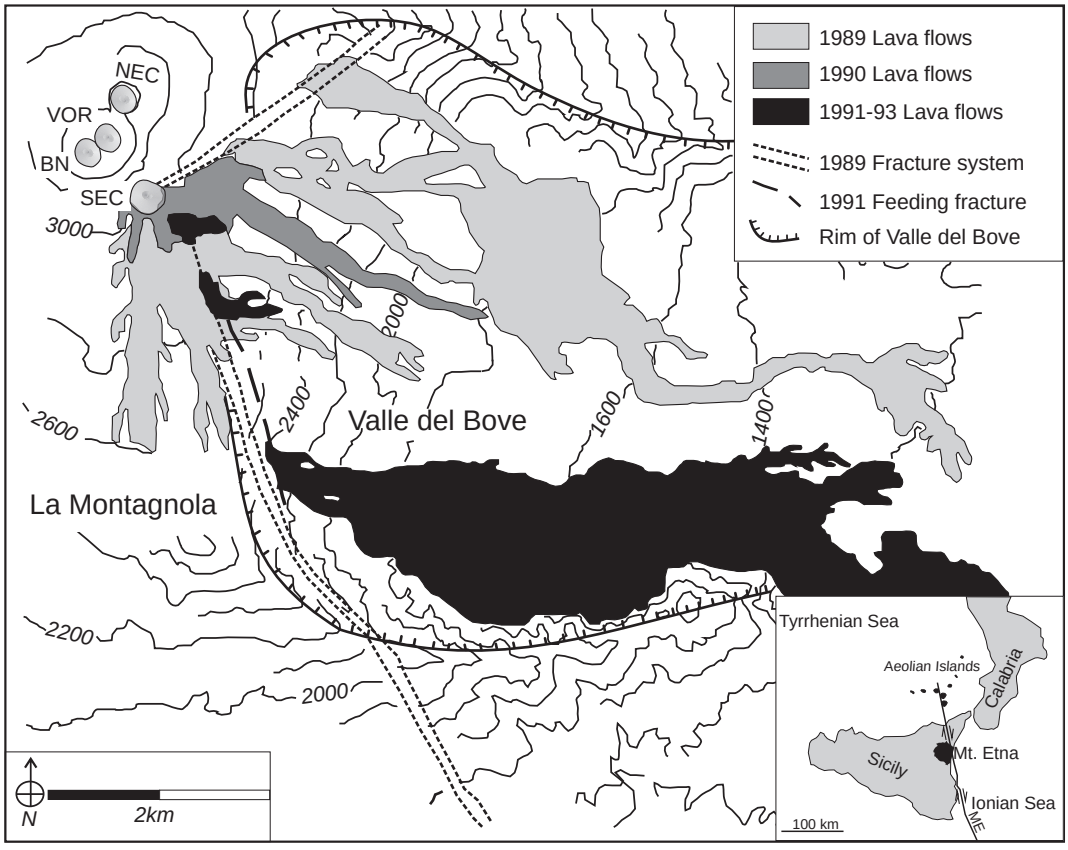

Fig. 1. 1991–1993 lava flow field map: Map of the SE-flank of Mt. Etna (Sicily) depicting the compound lava flow field of the major 1991–1993 flank eruption (black) and its predecessors in 1989 (light gray) and 1990 (dark gray). Figure modified from Barberi and Villari, 1994.

Table 1
Eruption chronology between September 1989 and March 1993.

Year	Onset	Duration (days)	Location and elevation (m a.s.l.)	Max length of flow field (km)	Eruption volume ($\times 10^6$ m^3)	Mean eruption rate (m^3 s^{-1})	Type of eruption
1989	11 Sep	16	SEC; 300–1900	2	12.2	8.3	Explosive
1989	27 Sep	12	E, NE flank; 2640/2550–1100	7.6	26.2	24.3	Mostly effusive
1990	4 Jan	<1	SEC; 3100–3000	0.2	20	–	Explosive
1990	12 Jan	<1	SEC; 3100–2700	1.5	0.3	–	Explosive
1990	15 Jan	<1	SEC; 3100–2000	2.5	1.2	–	Explosive
1990	1 Feb	<1	SEC; 3100–2100	2	0.5	–	Explosive
1991–1993	14 Dec	472	E, SE flank; 3100–2200	8.5	231 ± 29[a]	5.8[b]–12.3[c]	Effusive

Table from Tonarini et al. (1995); SEC: South East Crater.
[a] Eruption volume from Stevens et al. (1997).
[b] GPS data from Calvari et al. (1994).
[c] Field measurements from Barberi et al. (1993).

3. Petrographic observations and olivine zoning types

All samples display a porphyritic and scoriaceous texture containing the common Etnean phenocryst assemblage of plagioclase, clinopyroxene, olivine, and Ti-magnetite. The fine-grained and hyalopilitic groundmass consists mainly of the same mineral assemblage. Plagioclase (An87-42 - Armienti et al., 1994) is the most abundant phenocryst (9–12 vol.%) and contains numerous oscillatory zones, resorption surfaces, and many crystals show a sieved texture. Augitic clinopyroxene (Wo 50–43, En 43–33, Fs 17–10 — Armienti et al., 1994) is mainly euhedral (6–8 vol.%), with sector zoning and inclusions of magnetite and rarely olivine. Olivine (ca. 2–3 vol.%) is subhedral or anhedral, with crystals attaining 700 μm of size (see CSD in Armienti et al., 1994). Rare macrophenocrysts of up to 1.5 cm were also found. No significant differences in textures or modal compositions were found between the three different samples.

3.1. Olivine compositions and zoning profiles

Detailed concentration profiles (major and minor elements: Si, Fe, Mg, Mn, Ca, Ni) were measured along different directions in 57 olivine crystals, with a spacing varying between 3 and 10 μm between individual points. Data were acquired using the electron microprobe [and the secondary ion mass spectrometry (SIMS) for P measurements; see analytical techniques in Appendix A1 for details of both]. In addition, two-dimensional X-ray distribution maps of Fe, Mg and Ca were obtained for 18 olivine crystals, and a map of P distribution in one crystal, using the electron microprobe. The orientation of the crystallographic axes of analyzed olivine crystals were also determined using electron backscatter diffraction (Appendix A1 for more details).

Olivine composition varies between about Fo70 and Fo83 [Fo = 100 Mg/(Mg + Fe), in mol%]. Frequency histograms (Fig. 2a and b) of core and rim compositions show that there are four main types of core crystal populations, at Fo70-71, Fo72-75, Fo75-78, and Fo79-83. The rim compositions of the majority of the analyzed olivine crystals (77%) are between Fo72-75, with some rare crystal rims having compositions between Fo76-80 (Fig. 2b). The only compositional difference that we have found in the olivine from the three samples is that the most mafic crystals (Fo>81) are only found in the earlier part of the eruption (sample 14-December-1991). This probably indicates a decreasing contribution of mafic magma with time (see later). Core to rim traverses show that many crystals are characterized by compositional plateaus at their cores and sometimes also at the outer or intermediate zones (Fig. 3). Moreover, crystals can be normally zoned (Fo decreasing from core to rim), reversely zoned (Fo increasing from core to rim), or have an intermediate pattern of reverse zoning before being normally zoned at their outermost rims. An important observation is that the variability of the range (Fo 69 to 83.5 at core vs. Fo70 to Fo81 at rims) and distribution (Fig. 2) of compositions of olivine cores is significantly larger than that of the rims. We interpret these observations as evidence that the magmas that fed the 1991–1993 eruption were the result of interactions between at least three batches (recorded in the compositional histograms, in the zoning patterns and in the compositional plateaus seen in the traverses) that were mixed to variable degrees. We elaborate this hypothesis in more detail in the following sections.

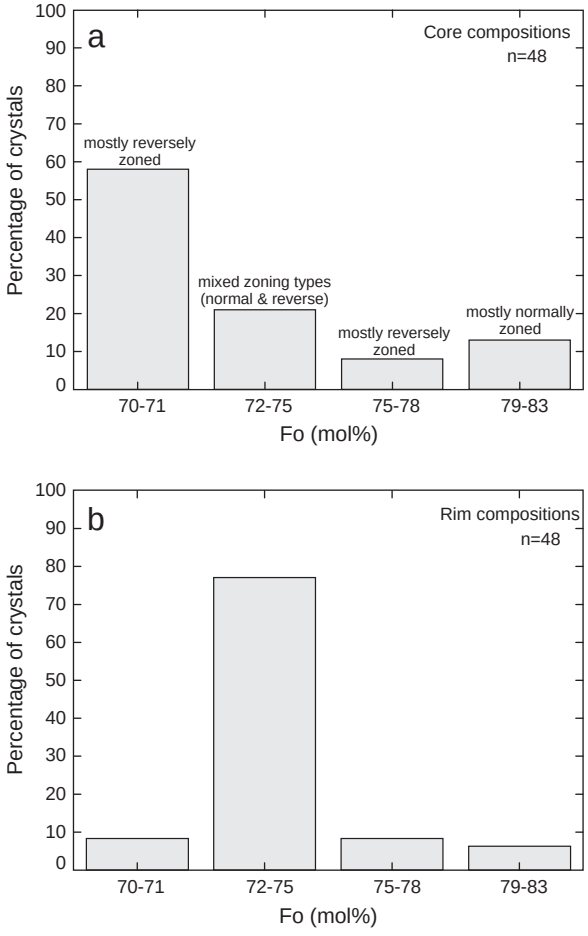

Fig. 2. Olivine compositions: Histograms of olivine core (a) and rim (b) compositions of 48 olivine crystals from the December 1991 – March 1992 eruption products. Note the diversity of core compositions that is absent in the rim compositions. Consideration of different populations of core compositions with associated zoning profiles allow three main reservoirs (M_0, M_1 and M_2) and one mixing reservoir (mm_1) to be identified.

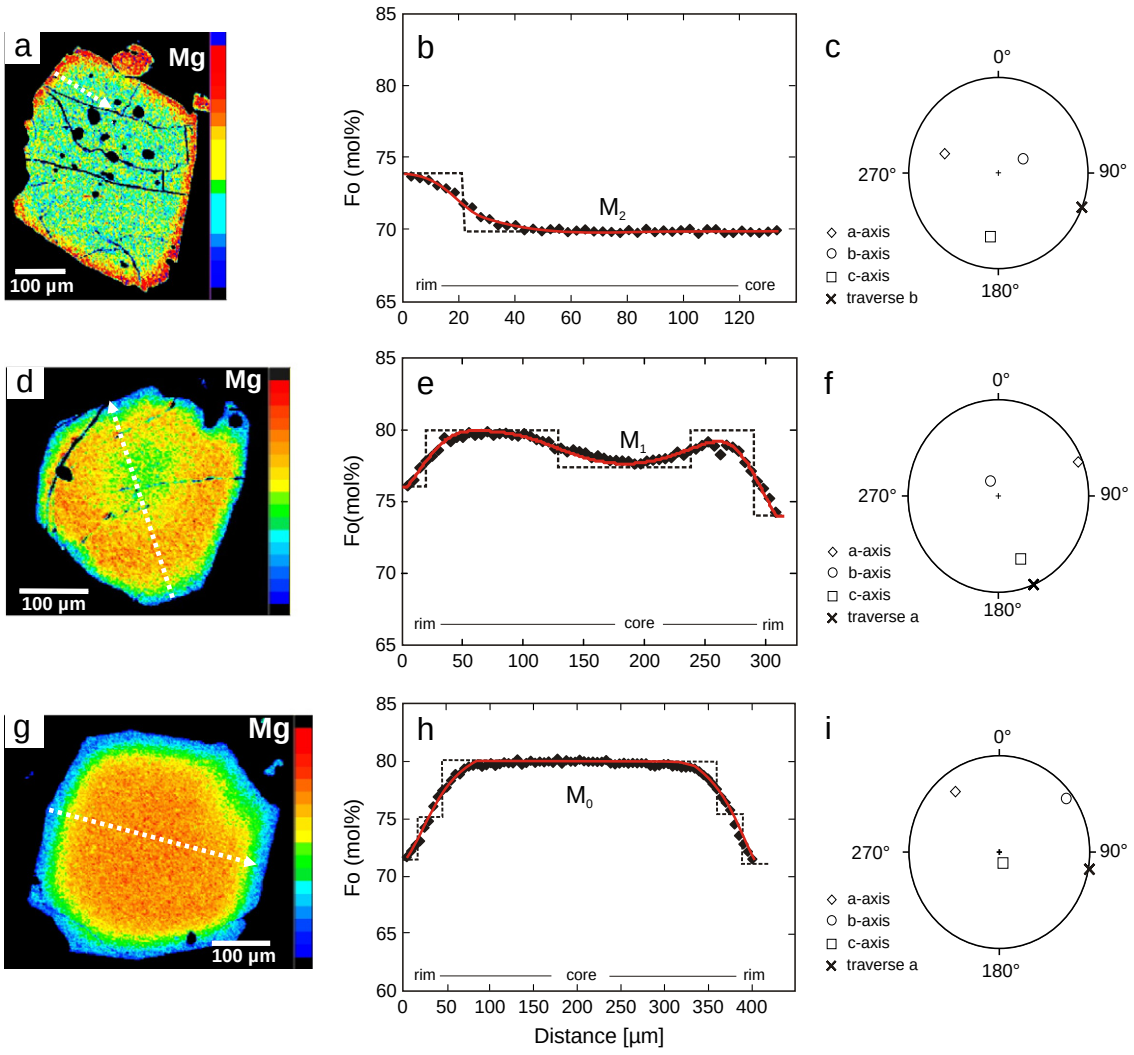

Fig. 3. (a-i) Element distribution maps, concentration profiles with model fits, and orientation data: Two-dimensional Mg distribution maps (a, d, g) of representative olivine crystals from the three identified olivine populations. White arrows indicate the directions of the electron microprobe traverses. (b, e and h): Black diamonds are measured analyses along the white lines in (a, d and g), showing concentration profiles from rim to rim or rim to core for Fo [Fo = 100 Mg/(Mg + Fe), in mol%]. Black dashed lines indicate the inferred initial profile shapes before diffusion occurred. Red lines are best fit diffusion models for the observed zoning profiles. M_0, M_1 and M_2 indicate growth in distinct magmatic environments as derived from the different core plateau compositions. (c, f and j): Stereographic plot on the lower hemisphere showing the angular relations between the major crystallographic directions (a-, b- and c-axis) in olivine and the directions of the electron microprobe traverses.

4. Determination of temperature and oxygen fugacity of equilibration

Analyses at the contacts between adjacent olivine and clinopyroxene crystals and between olivine and Ti-magnetite crystals were performed in order to estimate magmatic temperatures and oxygen fugacity (fO_2). Using the Fe–Mg olivine–clinopyroxene exchange geothermometer of Loucks (1996) we obtained temperatures of 1070 ± 20 °C for the 14 December 1991 and the 03 January 1992 samples and of 1090 ± 12 °C for the 14 March 1992 (see Fig. A2 in appendix). These temperatures overlap with the high end of the direct temperature measurements at the lava flows (1080–980 °C, Calvari et al., 1994). The fO_2s were determined using the QUILF algorithm of Andersen et al. (1993) using the compositions of coexisting olivine and Ti-magnetite. We used an activity of SiO_2 of 0.33 based on calculations using the MELTS software (Ghiorso and Sack, 1995) at the temperatures of interest for the bulk compositions of our rocks. Although we are combining different thermodynamic data bases the calculations give us an order of magnitude estimate that the fO_2 is close to the Ni–NiO oxygen buffer, which is consistent with the absence of ilmenite in these rocks, with the experimental results of Metrich and Rutherford (1998) and with direct measurements at eruptive vents (Sato and Moore, 1973).

5. Magmatic history recorded in the chemical zoning

5.1. The chain of events — a systems analysis approach

The occurrence of several compositional plateaus between the rim and the core (Fig. 3) of crystals indicates that the compositional zonings were not produced by simple fractionation during growth (e.g. Costa et al., 2008). Instead, each plateau composition represents growth in a distinct magmatic environment. Occurrence of plateaus indicates that effects of local magma dynamics (e.g. development of boundary layers) were averaged out during the timescale of growth of the relevant zones of the crystals. It also indicates that residence times in the given environments were long enough to be recorded by crystal growth (e.g. see Ruprecht et al., 2008). Clearly, passage of crystals through environments at a rate that is faster than crystal growth rates would result in no records of such environments being preserved in the zoning record. Consideration of the core plateau compositions

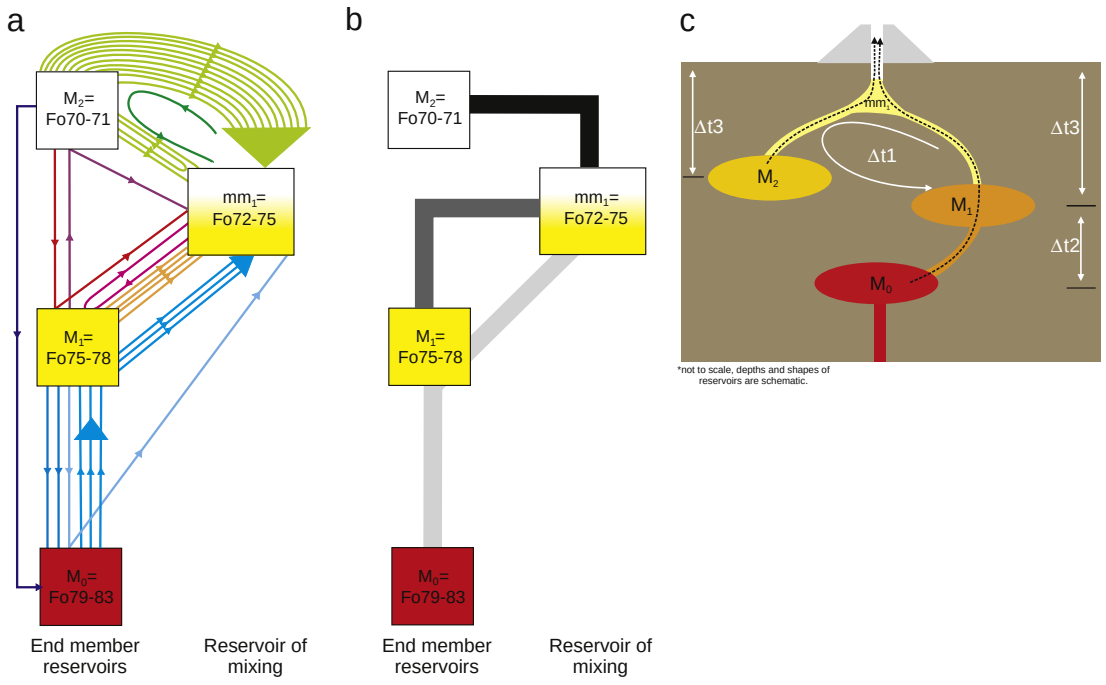

Fig. 4. The plumbing system: (a) Simplified systems analysis of the zoning patterns recorded in olivine crystals erupted between December 1991 and March 1992. Each box represents a magmatic reservoir of different composition identified by the overall core plateau compositions and zoning patterns. M_0, M_1 and M_2 represent end member reservoirs (M_0 = Fo79-83, M_1 = Fo75-78 and M_2 = Fo70-71), whereas mm_1 is a reservoir of mixing. The colored lines represent the zoning patterns recorded in single olivine crystals. The arrows indicate the direction of the zonings from core to rim. All reservoirs are connected with each other. The density of the connection lines can be used to infer the dominant passageways of magma transport. (b) Information distilled from (a) to highlight the three main magma pathways M_0–M_1–mm_1 (light gray bar) M_1–mm_1 (dark gray bar) and M_2–mm_1 (black bar). (c) An example of a physical plumbing system that is consistent with (a) and (b). Other possibilities exist. Locations and connectivity of reservoirs are time integrated, at any given time one or more of these may not have existed. Black dotted lines mark the preferred path followed by many crystals. Various timescales (Δt_1, Δt_2 and Δt_3) that can be extracted from kinetic modeling relate to duration of residence of melts in different segments of the plumbing system, as shown here.

with the various zoning patterns of the four olivine groups (Fig. 2) indicate growth in four different magmatic environments (ME) which are hereafter referred to as M_0 (= conditions where Fo79-83 olivines form), M_1 (= Fo75-78), M_2 (= Fo70-71) and mm_1 (= Fo72-75) (Fig. 3). Assuming that crystal growth occurred sequentially from core to rim, we hypothesize that the compositions at the rim record the latest environment/events (i.e. immediately preceding eruption) shared by all crystals in a given flow, while compositions in the interior of a crystal record progressively older environments/events experienced by the crystals. Thus, the chemical stratigraphy recorded in the compositional zoning patterns can be used to track the evolution of different packages of melt through distinct magmatic environments (ME). However, the patterns of zoning (i.e. sequences of recorded events / environments) are so diverse between crystals that a simple interpretation is not possible.

To analyze the complex diversity, we have plotted the data in a Systems Analysis sense. [A system is a combination of elements that act together to accomplish an objective. Systems analysis aims to study how the connections between the elements influence the overall behavior of the system. (Palm, 2005)]. The complete set of compositional data of olivines can be represented by considering the three distinct core composition groups (M_0, M_1 and M_2) in combination with the additional group that is intermediate and can be produced by mixing of these ($M_1 + M_2 = mm_1$) (Fig. 4a). Compositional zoning within an olivine crystal can then be depicted by a directed line that begins at the ME corresponding to its core composition (e.g. M_0, M_1 or M_2), passes through successive ME's recorded from core to rim and terminates at the ME represented by the rim composition. Each crystal can be represented by one such evolution line, and each sequence of ME's (i.e. a given type of evolutionary history of a crystal/melt package e.g. M_0–M_1–mm_1) is shown using a different color (Fig. 4a). Such an analysis reveals that in spite of the complex diversity of zoning patterns, certain evolutionary tracks are prevalent in the history recorded by the olivine population (Fig. 4a). The range of colors in this Systems connectivity diagram indicates that although all ME's may be connected to each other in various sequences, a vast majority of crystals tracked the history M_0–M_1–mm_1, M_2–mm_1, and M_1–mm_1 (Fig. 4b). A different, wavelet based phylogeny approach for determining progressive shared environments of intensive and extensive variables recorded in chemical zoning of a population of crystals has been developed by Wallace and Bergantz (2002, 2004, 2005). This numerical tool is well suited for applications to minerals such as plagioclase that record a larger numerical range of compositions that have been largely unmodified by diffusion.

The magmatic environment (ME) that is recorded by the composition of a crystal can change because of a change in any one or more of the relevant intensive thermodynamic variables such as temperature, pressure, oxygen fugacity, water content, or melt composition. The latter can be due to multiple processes e.g. local variations around a crystal caused by crystal fractionation/diffusion, or larger scale variations caused by magma mixing/input of new melts to a reservoir. Different ME's can also be different segments of the same physical magma reservoir with different crystal:melt ratios. However, the simplest situation that can produce distinct compositional populations rather than a continuous evolution is where crystals experience distinct physical environments due to movement of melt from one reservoir to the next; each reservoir with its own ME. We have chosen to interpret the ME's recorded by olivines in this study in this context. According to this interpretation, M_0, M_1 and M_2 would represent three different melt reservoirs (i.e. components of a magma mush zone) whereas mm_1 would be compositions produced by mixing in the connector between M_1 and M_2. Such connectors could be permanent or transient and the patterns of compositional variation can be rationalized in terms of a

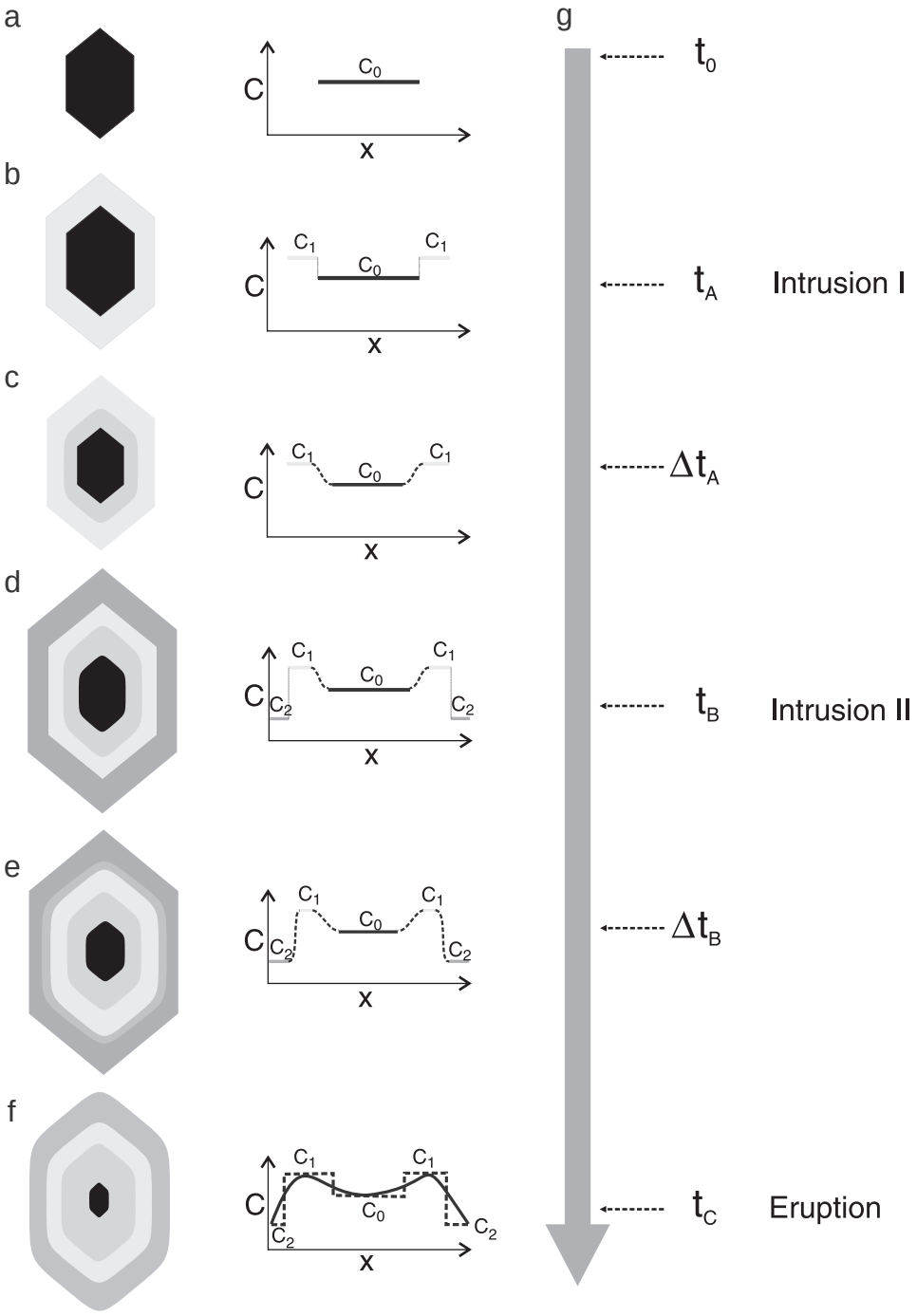

Fig. 5. Conceptual illustration of sequence of events and sequential residence times, as reflected in the compositional zoning of crystals. (a) Initially homogeneous crystal (C_0) at time t_0; (b) The intrusion of a new batch of melt at t_A causes the formation of a new compositional plateau C_1. (c) The concentration gradient between the two compositional plateaus, C_0 and C_1, sets up a diffusive flux which starts to smooth the initial concentration profile. (d) At time t_B a second intrusive event changes the local thermodynamic conditions and initiates the formation of a second plateau, C_2. (e) Concentration gradients between C_0, C_1 and C_2 induce diffusive fluxes that strive to homogenize the entire concentration profile. (f) Rapid cooling during eruption freezes the diffused concentration profile (black continuous line). Black dashed line indicates the 'initial' concentration profile that would be observed if no diffusion had occurred. X: Distance. (g) Time line depicting chronology of magmatic events. Δt_A and Δt_B indicate the duration of diffusion at different stages before eruption — these are the quantities that can be retrieved by modeling observed concentration profiles.

multistage history of magma mixing in different reservoirs before eruption. This interpretation allows the Systems connectivity diagram to be translated to a magma plumbing system, and the one commensurate with the sequence of ME's found for olivines observed in this study is shown in Fig. 4c. We derive from this that the interaction between reservoirs M_0 (= Fo79-83) and M_1 (= Fo75-78) was followed by melt movement from M_1 to the main reservoir M_2 (= Fo70-71) with mixing in a connector reservoir mm_1 (= Fo72-75). The large number of crystals depicting the history M_2–mm_1 indicates that these two reservoirs had been in communication for some time and that mixing between these two kinds of melts was widespread. Fig. 4c is thus a re-creation of the favored plumbing system that fed the first months of the

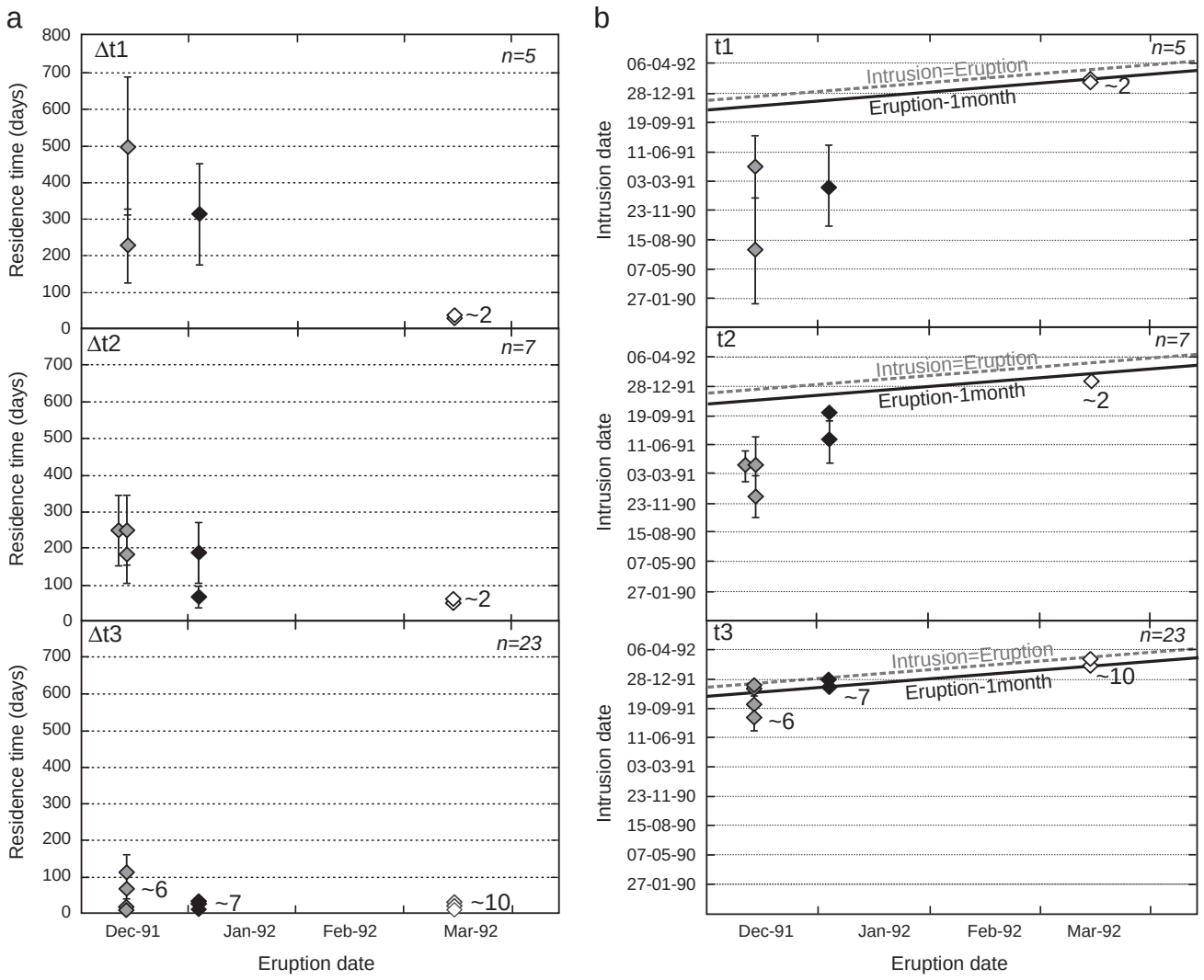

Fig. 6. Residence and Intrusion times: (a) Calculated residence times (days) vs. eruption dates of the studied lava samples. Identification of three groups of residence times (Δt_1, Δt_2 and Δt_3) obtained from different kinds of zoning profiles. (b) Intrusion times vs. eruption dates. Intrusion were times obtained by successively subtracting the residence times (Δt_1, Δt_2 and Δt_3) from the known eruption dates. The three groups of intrusive events indicate magma intrusions at different points of time. Each point in the plots represents the average of up to six determinations (multiple elements and crystallographic directions) for individual olivine crystals. Error bars account for the uncertainties from geothermometry (i.e. December 1991 and January 1992 1070 ± 20 °C; March 1992 1090 ± 12 °C). Multiple overlapping points are shown slightly offset from each other, with the number of overlapping points indicated on the side. Gray stippled line: Date of Intrusion equals date of eruption i.e. points on these lines would indicate that intruded magma was erupted immediately without significant residence. Black line: Eruption date minus one month i.e. points on a line such as these would indicate a residence time of one month in the reservoir before eruption.

1991–1993 flank eruption. The distinction in olivine compositions produced in these different reservoirs could result due to variation of any combination of the thermodynamic intensive variables noted above.

5.2. The temporal information

As crystals track a multistage evolution history such as the ones noted above at high temperatures, chemical diffusion operates to erase the concentration gradients produced. This is schematically illustrated in Fig. 5. The approach assumes that crystal growth rates are much faster compared to elemental diffusion rates within crystals. This is consistent with known rates of these two kinds of processes and model calculations (e.g. Costa et al., 2008). If diffusion coefficients for the elements concerned are known at the relevant conditions then the extent of compositional homogenization provides a measure of the timescale of residence in different ME's. Some of the processes of transfer of crystals to different environments could result in crystal dissolution and ignoring that could potentially falsify the residence time information that is extracted from diffusion modeling of compositional zoning. We have devised criteria that allow crystals affected by significant non-diffusional modification of compositional zoning to be identified (Costa et al., 2008, also see below), and such crystals are not used for the extraction of temporal information.

The novelty in the modeling technique applied in this work arises from the stepwise simulation of the observed profiles. Compositional plateaus are produced instantaneously at different stages according to the sequence of events inferred from the Systems analysis for the concerned crystal (at points of time t_i, e.g. t_A, t_B in Fig. 5). These concentration gradients are allowed to relax diffusively during the time period between each such growth stage ($=\Delta t_i$ e.g. Δt_A, Δt_B in Fig. 5), up to the point of final eruption, such that the final calculated profile matches the observed one (see Fig. 3b, e and h). Therefore, different sections of the crystal experience diffusion for different durations. The

parts near the core experience the longest periods of diffusion ($\Delta t_A + \Delta t_B + ...$etc.) whereas compositions near the rim were often produced by the very last events before (or even during) quenching and have had little time for diffusive modification. For each successive stage, the partially modified profile from the previous stage is taken to be the initial concentration distribution. Therefore such stepwise simulation of profiles in a crystal population allows the residence times of the crystals in different sections of the plumbing systems to be determined separately, providing a complete spectrum of timescales that describe the dynamics of the passage of melts through the plumbing system.

6. Modeling the compositional gradients in olivine

6.1. Diffusion equation and diffusion coefficients

The diffusive modification of compositional zoning patterns recorded in olivine crystals can be described by Fick's second law:

$$\frac{\partial C_i(x,t)}{\partial t} = \frac{\partial}{\partial x}\left(D_i \frac{\partial C_i(x,t)}{\partial x}\right) \quad (1)$$

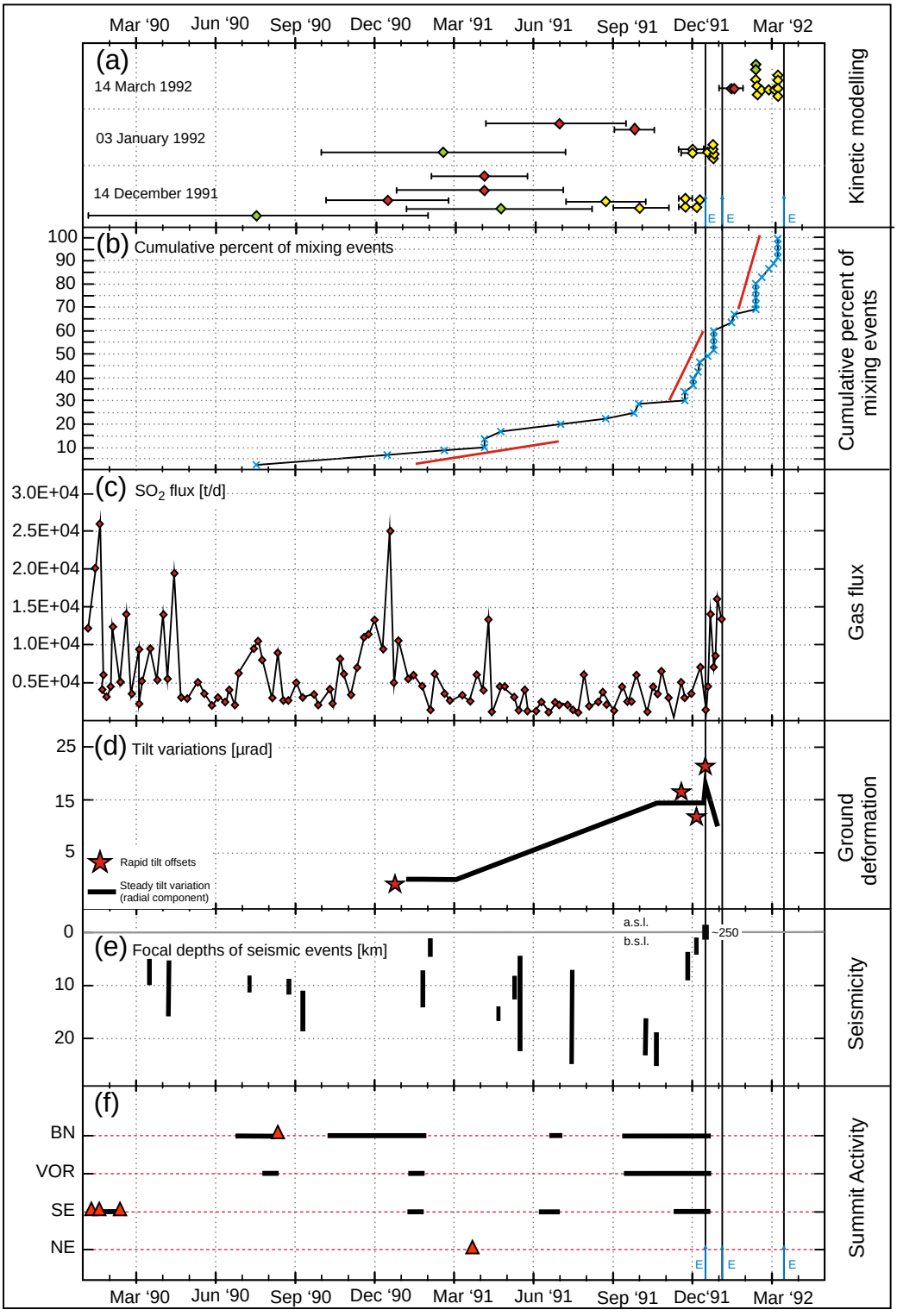

where C_i is the concentration of element i, x is the distance, D_i is the diffusion coefficient of element i and t is the time. The evolution of the concentration with time (t) at different spatial coordinates (x), C_i (x, t), is obtained numerically using a one dimensional finite difference scheme. The two dimensional X-Ray maps (Fig. 3) reveal that one-dimensional calculation of diffusion along a profile is adequate. Diffusion in olivine is anisotropic and the diffusion coefficients used in the calculations need to be obtained for the relevant crystallographic direction. Knowing the diffusivities along the principal crystallographic axes, diffusion rates along any arbitrary crystallographic direction along which profiles have been measured can be obtained (e.g. see Costa and Chakraborty, 2004 for an example of such calculation in olivine).

6.2. Initial and boundary conditions

The initial conditions refer to the shape of the zoning pattern before diffusive modification. Different strategies were adopted to identify the initial conditions for different kinds of profiles:

(i) The plateau compositions at cores of larger crystals are widely unaffected by diffusion (as there is no gradient) and thus they preserve the initial composition. In the olivine crystals investigated in this study, extended core plateaus in the compositional range defined by the reservoirs M_0, M_1 and M_2 could be identified (see above), and where possible, these compositions were used as initial plateaus (Fig. 3b and e).
(ii) Finding the appropriate initial conditions for the crystal rims is slightly more complex. In many cases, plateaus at or near the rims are preserved. These can be used to infer the initial profile shapes (Fig. 3b). Use of the main reservoir compositions identified above (M_0, M_1, M_2, and mm_1) to describe the initial conditions for plateaus at different stages was found to yield consistent results. There was no need to invoke arbitrarily chosen plateau compositions.
(iii) In cases of normally zoned concentration (i.e. decreasing Fo contents from core towards the rims) profiles (Fig. 3c) the estimation of the initial profile shape is less straightforward. We were guided by the restricted set of reservoir compositions and comparison with zoning profiles of slower diffusing elements such as P (see Appendix Fig. A3; Millman-Barris et al., 2008). Weak modification of Ca profiles can also help to infer the initial zoning patterns of faster diffusing divalent cations (e.g. Fe–Mg, Ni and Mn) (Costa et al., 2008).

The crystal boundaries were considered to be open and in communication with an infinitely large (relative to diffusion length and time scales) melt reservoir. A no flux boundary condition was imposed by symmetry at the cores with plateau compositions. The choice of initial profile shapes and rim compositions at the boundary were different for each crystal, dictated by the specific evolutionary path the crystal tracked (Fig. 4a).

6.3. Diffusion coefficients

Diffusion coefficients in olivine are known for Fe–Mg, Ni, Mn and Ca as functions of temperature, pressure, composition, oxygen fugacity and crystallographic direction from experimental measurements (Coogan et al., 2005; Dohmen and Chakraborty, 2007; Petry et al., 2004). These were combined with our temperature, and fO_2 determinations and the orientation of the crystallographic axis to obtain the appropriate diffusion coefficient for the simulation of each concentration profile.

6.4. Robustness criteria for determination of time scales

To avoid modeling concentration profiles that are mainly the result of processes other than diffusion (i.e. growth or dissolution) the following criteria were applied:

(i) In general, two electron microprobe traverses were measured across each olivine crystal. If modeling of both profiles did not yield the same time constraints consistent with known diffusion anisotropy, the concentration profiles were considered to be affected by processes other than diffusion and were not used for extracting timescales by diffusion modeling (Costa et al., 2008).
(ii) Concentration profiles of multiple elements (Fe–Mg, Mn, Ca and Ni) with different diffusivities were measured. If modeling of these profiles did not yield the same times within uncertainty the results were also not considered as reliable.
(iii) Two-dimensional element distribution maps helped to identify true diffusion zoning patterns (Costa et al., 2008; Costa and Dungan, 2005). According to the diffusion anisotropy the width of the zonings may be distinct in different crystallographic directions, depending on the plane of the section. Thus, olivine crystals where concentration gradients have been produced by diffusion can be selected in advance in many cases.
(iv) Results obtained from multiple crystals that experienced the same evolutionary history were required to be consistent with each other.

The discussion below is based on results that fulfill these criteria. Up to 28 such crystals were found in this study from which we obtained 35 independent time estimates (Table 2) of different magmatic processes. The fact that the number of determinations of durations of events is smaller than the total number of crystals studied (57) is because, (a) not all crystals were significantly zoned and (b) not all zonings were suitable for diffusion modeling.

7. Timescales of processes in the plumbing system

Examples of model calculations that fit the observed profile shapes from different eruptions are shown in Fig. 3b, e and h. The retrieved time scales (Fig. 6) provide a number of insights into the nature and the behavior of the plumbing system before and during the 1991–92 eruptions of Mt. Etna. Fig. 6a summarizes the calculated residence times

Fig. 7. Connection of timescales from kinetic modeling to monitoring data: (a) Calculated times at which intrusion occurred to different reservoirs, as inferred from kinetic modeling of investigated eruption products (14 December 1991, 03 January and 14 March 1992). Green diamonds: Intrusive event t_1; Red diamonds: Intrusive event t_2; Yellow diamonds: Final intrusion t_3. Error bars represent uncertainties from various sources, as discussed earlier. (b) The cumulative percent of events recorded (in compositional zoning of olivine) up to any given time before eruption if the total number of recorded mixing/melt movement events is scaled to 100. Black line: Cumulative curve, Symbols (blue asterisks): Timing of individual events, Red lines: Slopes of the cumulative curve at different segments. Changes in slope in this plot indicate the activation of newer regions of the plumbing system or changes in the rates of melt movement/mixing. Consistent with our analysis, three such regions can be clearly demarcated. Combined consideration of data from panels (a) and (b) show how mixing/movement in multiple reservoirs are active simultaneously in a plumbing system such as this. Panels (c–f) show various precursory signals monitored in the year before the onset of the 1991–1993 SE-flank eruption. (c) SO_2 flux signal from Caltabiano et al. (1994). (d) Continuous and rapid variations of the radial tilt component at the surface in the immediate vicinity of the eruption region (Bonaccorso et al., 1991; Bonaccorso et al., 1994). (e) Depth distribution pattern of seismic foci (Patanè et al., 1994; Patanè and Privitera, 2001). (f) Summit activity in 1990–1991. Thin dotted line: Continuous degassing; Thick black line: Strombolian activity, intracrater lava flow(s); Red triangle: Strong strombolian explosions/fire fountain episodes. BN: Bocca Nuova crater; VOR: Voragine crater; SE: South-east crater; NE: North-east crater (Calvari et al., 1994). Note that the thick black lines appear at the time when the cumulative mixing curve in (b) begins to rise, and that the first change in slope of the cumulative curve corresponds to the point of time of appearance of multiple thick black lines occurring simultaneously in panel (f) (and initiation of progressive shallowing of seismic foci in panel (e)). The vertical black lines cutting across all panels and the blue arrows show the timing of the three eruptions on 14 December, 1991, 03 January, 1992 and 14 March, 1992.

as a function of eruption dates of the corresponding lava samples. It was found that the residence and the transit of these olivine crystals between different reservoirs of the 1991–1993 plumbing system occurred over three characteristic time scales — Δt_1, Δt_2 and Δt_3 (Figs. 4b and 6a):

(i) The calculated residence times Δt_2 were mainly obtained from crystals that tracked melt transfer between M_0 (Fo79-83) and M_1 (Fo75-78) and this transfer occurred around 3–6 months before eruption onset (Fig. 6a).
(ii) By contrast, the residence time Δt_3 is much shorter and lasted less than a month (Fig. 6a). This timescale is characteristic for the melt transfer and mixing between M_1–M_2–mm_1. The rather short timescales of this final mixing process can be confirmed in all eruption products.
(iii) The last group of timescales (Δt_1) is related to a minor population of crystals (Table 2) that cycled between multiple reservoirs before getting incorporated in the final eruption products. These crystals are heterogeneous in their recorded times and some of them record the oldest histories ranging back to a year and a half (Fig. 6a).

Knowing the residence times of melt packages in different reservoirs, it is possible to calculate the dates of intrusion of these melts into different reservoirs by successively subtracting the residence times from the known eruption dates of the investigated lava samples (Fig. 6b).

7.1. Combination of chemical stratigraphy and kinetic modeling — chronology of magma transfer

Combination of the information recorded in the chemical stratigraphy of compositionally zoned olivine crystals and the temporal information from modeling the modified zoning profiles allows reconstruction of the chronology of the passage of a body of magma between different reservoirs (Fig. 4c):

(i) The first significant event recorded in the olivine crystals is the early mixing (t_2) between the more mafic M_0 (=Fo79-Fo83) and the intermediate M_1 (=Fo75-78) magma in December 1990 (Fig. 6b).
(ii) Subsequently, this magma started to migrate into the last (more shallow) sections of the plumbing system by August–September 1991 (t_3), in order to mix with the dominant M_2 (=Fo70-71) melt. If the number of crystals showing evidence of a given melt transfer event is an indication, then the input of melt in the final segment of the plumbing increased notably after September 1991 (Fig. 6b). It is possible that this final mixing eventually triggered the initiation of the 1991–1993 eruption. The early eruption products of December 1991 carried many olivine crystals that record both of these mixing events (at t_2 and t_3) (Fig. 6).
(iii) As the eruption sequence evolved from January towards March 1992 the amount of crystals recording the initial mixing event (at t_2, M_0 and M_1) decreased progressively (Fig. 6), indicating that the supply of the more mafic magma (M_0) decreased significantly with time. This agrees with petrologic monitoring results that show a sharp decrease in the Mg number for rocks erupted after December 24, 1991 (Tonarini et al., 1995).
(iv) Once a preferred pathway for magmas was established, residence within the different sections of the plumbing system decreased considerably. From January towards March 1992 the plumbing system had been flushed enough so that the residence times of melts in the corresponding segments was only about a month or less (Fig. 6).
(v) Finally, the characteristically longer time scales (Δt_1) recorded by rare olivine crystals (Fig. 6) that circulated through multiple reservoirs before being incorporated in an eruption product indicates that connectivity between reservoirs are more long lasting than the average residence times of magma batches in these reservoirs. This does not, however, exclude the possibility that such connectivity may be periodic (e.g. opening and closing by propagation of dikes) rather than continuous.

Table 2
Summary of modeling results and sequence of reservoirs as recorded in compositionally zoned olivine crystals.

Sample	Olivine	Sequence of reservoirs	Δt1 (days)	Δt2 (days)	Δt3 (days)
14-Dec-91	Ol-13	M0 + M1 + mm1	–	184	73
	Ol-4a	M1 + M0	–	250	–
	Ol-10	M1 + M0 + mm1	–	250	113
	Ol-3	M2 + mm1	–	–	17
	Ol-4b	mm1 + M1	–	–	8
	Ol-2	mm1 + M2 + mm1	229	–	8
	Ol-14	M1 + mm1 + M1	500	–	17
03-Jan-92	Ol-4	M1 + M0	–	188	–
	Ol-9	M0 + M1 + mm1	–	67	34
	Ol-2a	M2 + mm1	–	–	8
	Ol-2b	M2 + mm1	–	–	8
	Ol-10a	M2 + mm1	–	–	33
	Ol-15	M1 + M2 + mm1	313	–	6
	Ol-14	M2 + mm1	–	–	8
	Ol-10b	M2 + mm1	–	–	17
14-Mar-92	Ol-12	M1 + mm1	–	58	—
	Ol-10a	M0 + M1 + mm1	–	52	8
	Ol-1	M2 + mm1	–	–	30
	Ol-3	M2 + mm1	–	–	8
	Ol-7	M2 + mm1	–	–	25
	Ol-6	M2 + M1 + mm1	29	–	–
	Ol-9	M2 + mm1 + M2	–	–	9
	Ol-10b	M2 + mm1	–	–	15
	Ol-11	M2 + mm1	–	–	12
	Ol-13	M2 + mm1 + M2	–	–	9
	Ol-2	mm1 + M1	–	–	32
	Ol-5	mm1 + M1	–	–	30
	Ol-8	M2 + M0	29	–	–

In summary, the widespread (t_3) events corresponding to the melt transfer/mixing history M_1–M_2–mm_1, which are recorded in all investigated eruption products occurred mainly after September 1991. The less common and earlier melt transfer between M_0–M_1 occurred after December 1990 until close to the eruption onset (Fig. 6b). Some rare crystals record processes from the middle of 1990 (t_1) (Fig. 6 and Table 2). The timescales we obtain range between a few days (Δt_3) and 2 years (Δt_1) — a range that is widely consistent with the active nature of Mt. Etna and indicates that the shallowest reservoirs are regularly emptied and replenished by input of new magma (see also Albarède, 1993).

8. Connecting timescales from kinetic modeling to monitoring data

This scenario of melt transfer and evolution of the plumbing system that fed the first months of the 1991–1993 flank eruption may now be linked to various monitoring signals that were recorded before the eruption sequence began (Fig. 7). The 1991–1993 flank eruption was preceded by numerous signals (e.g. Barberi and Villari, 1994). A long-term inflation of the volcanic edifice was recorded during the 10 years before the eruption onset (Bonaccorso, 2001; Bonaccorso et al., 1994). The year immediately preceding the eruption was marked by many middle- to short-term precursor signals. Fig. 7 is a composite depiction of several relevant geophysical (seismic, and ground deformation signals), and geochemical (SO_2 gas flux) monitoring data. Additionally, the summit activity, a direct expression of magmatic activity at depth, in the period from January 1990 until eruption onset in December 1991, is shown (Fig. 7f).

At the end of 1990 and in early 1991 an increase of summit activity and influx of lava in three (i.e. Bocca Nuova, Voragine and SE-crater) of the four summit craters was observed (Fig. 7f) (Calvari et al., 1994). The blazing summit activity was preceded by a sharp deformation signal (Fig. 7d) recorded at all stations accompanied by a prominent peak of SO_2 degassing (Fig. 7c) (Bonaccorso et al., 1991; Caltabiano et al., 1994; Calvari et al., 1994). The simultaneous occurrence of the tilt offset at all stations indicates that the cause was a deep rather than a shallow and localized event. This coincides with the rather shallow focal depth of the following seismic swarm in February–March 1991 (3 to 9 km b.s.l.; Patanè et al., 1994). In the same period (March–April 1991) the filtered CO_2 soil degassing signal (not shown in Fig. 7) also displayed a prominent peak (Giammanco et al., 1995). Since March 1991, a gradual increase of the radial tilt component (mainly detected by the tilt station CDV; Bonaccorso et al., 1994) could be observed and finally this attained a maximum in October, a few weeks before a new uplift heralded the 1991–1993 eruption onset (Fig. 7d).

Relating these observations to the reconstructed plumbing system and the proposed timescales of melt transfer within it, we find that the initial recharge of melt at depth (mid 1990) may have caused some of the melt already residing at shallower levels to circulate (time since that point recorded as Δt_1). This rarely recorded process can be interpreted either as a predecessor of the 1991–1993 eruption, or as a concluding spasm of the 1989 flank and the 1990 summit activities. The main melt transfer between M_0 and M_1 (time since then recorded as Δt_2) was seen since December 1990 and it coincides with a prominent SO_2 signal, a marked tilt offset, and the increasing Strombolian activity at three summit craters (Fig. 7). The final migration of melt into the last section of the plumbing system was observed since September 1991, and the time between this event and eruption was recorded as (Δt_3) in the olivine crystals. From September 1991 onwards, a continuous recharge of the final plumbing segment occurred. This observation matches with the increasing frequency and intensity of shallow seismicity (Fig. 7e). The hypocenters of seismic swarms become progressively shallower towards the eruption onset and were accompanied by several sharp tilt offsets.

The broad overall evolution of the plumbing system is seen more clearly in a cumulative plot of mixing events recorded in olivine crystals (Fig. 7b). Changes in slopes in such a plot record that (a) melt movement and mingling began increasing from about December 1990, (b) additional movement and mingling, involving newer levels of the plumbing system, as we are now able to decipher, was initiated around September 1991, and (c) a final increase in movement and migration occurred immediately before eruption. This last phase continued on after initiation of eruption on December 14, 1991, with melt mingling and flowing through the system rapidly (i.e. short residence times), sustaining the remarkably voluminous 1991–1993 eruption. The plot emphasizes that these events are cumulative and occur in parallel. This helps to highlight how it is difficult to isolate single causal phenomena in a complex interconnected plumbing system — the mixing that likely triggered the eruption (pre-eruptive mixing) also promoted and laid out the pathway for subsequent melt mixing (syn-eruptive mixing) and movement. However, we are now able to elucidate such complex evolutionary scenarios from the record preserved in compositional zoning in minerals.

The most striking aspect of this analysis is that the timing of initiation of both inferred mixing events (in December 1990 and September 1991) are marked by an observed increase of Strombolian activity and lava input in the summit craters (see Fig. 7f and its caption). This finding is perhaps the most robust indication that the timescales we obtain from kinetic modeling are related to movement of real batches of melt at depth, establishing this tool as a method that can be applied to situations where such close monitoring is not available.

9. Conclusions

We have developed a method to systematize diverse, apparently chaotic zoning patterns in volcanic minerals so that pathways taken by different packages of melt in a complex plumbing network may be tracked. Sequential kinetic modeling of such zoning patterns allows the timescales of residence and melt migration through the plumbing network to be inferred, providing a dynamic picture of the evolution of the plumbing system as an eruption cycle evolves. These results can be correlated with surface monitoring data, providing a connection between intensive thermodynamic variables recorded in the chemistry of melts and minerals and signals measured at the surface that are interpreted to be resulting from movement of melts at depth. The approach we have used is quite inexpensive and can be gainfully employed to understand the plumbing systems and their temporal evolution for geographically and temporally remote volcanoes. In this sense, collection of data such as the ones in this study can help to develop characteristic timescales of evolution for different kinds of volcanic plumbing systems. This may be particularly valuable for the study of dormant or weakly active volcanoes.

Application of this tool to the initiation of the voluminous 1991–1993 eruption sequence at Mt. Etna reveals that three timescales characterize the evolution. A longer timescale of about 6 months to a year and a half is recorded in a minor population of crystals and relates to circulation of melt batches through various pre-existing reservoirs. The two other timescales (a few days to a few months) relate to input and mixing of a mafic magma to a shallower reservoir, commencing in December 1990 (and coincident with the appearance of heightened summit activity), and to the main transfer of melt from this reservoir to the shallowest levels of residence before eruption (? conduit) beginning in September 1991. This latter melt movement may well have triggered the start of eruption in December 1991. Overall the short timescales recorded in different crystals are consistent with the extremely active nature of Mt. Etna, where shallower reservoirs are most likely regularly replenished (Corsaro and Pompilio, 2004; Patanè et al., 2008). In particular, we are able to resolve how these various processes keep occurring in parallel, providing a continuous gradation from pre-eruptive mixing with possible triggering effects to syn-eruptive mixing that lead to cleansing and refilling of plumbing systems.

Mt. Etna currently finds itself in the midst of a very active phase. The latest eruption cycle began in 2000 and has shown several interesting aspects e.g. simultaneous eruption at several locations and a change in the nature of the eruptive products (e.g. increase in volatile components). To the extent that major changes in plumbing systems of volcanoes as large as Mt. Etna do not occur overnight, the insights on the plumbing system gained from the 1991–1993 eruption may help to better evaluate, invert and understand the various monitoring signals from the current eruptive sequence.

Acknowledgments

We thank H.-J. Bernhardt (Bochum), J. Berndt-Gerdes (Münster) and R. Neuser (Bochum) for their assistance with the electron microprobes and with the electron backscatter diffraction (EBSD) analyses. We are grateful to T. Ludwig (University of Heidelberg) for the SIMS analysis. This work was funded by the German Science Foundation as part of the collaborative research center (SFB) on Rheology of the Crust — from the upper crust to the subduction zone (SFB 526). We thank G. Bergantz and an anonymous reviewer for very constructive reviews.

Appendix A. Supplementary data

Supplementary data to this article can be found online at doi:10.1016/j.epsl.2011.05.008.

References

Albarède, F., 1993. Residence time analysis of geochemical fluctuations in volcanic series. Geochim. Cosmochim. Acta 57, 615–621.

Andersen, D.J., Lindsley, D.H., Davidson, P.M., 1993. QUILF: a Pascal program to assess equilibria among Fe–Mg–Mn–Ti oxides, pyroxenes, olivine, and quartz. Comput. Geosciences 19, 1333–1350.

Anderson, A.T., 1984. Probable relations between plagioclase zoning and magma dynamics, Fuego volcano. Guatem. Am. Miner. 69, 660–676.

Armienti, P., Pareschi, M.T., Innocenti, F., Pompilio, M., 1994. Effects of magma storage and ascent on the kinetics of crystal growth. The case of the 1991–92 Mt. Etna eruption. Contrib. Miner. Petrol. 115, 402–414.

Barberi, F., Villari, L., 1994. Volcano monitoring and civil protection problems during the 1991–1993 Etna eruption. Acta Vulcanol. 4, 157–167.

Barberi, F., Carapezza, M.L., Valenza, M., Villari, L., 1993. The control of lava flow during the 1991–1992 eruption of Mt Etna. J. Volcanol. Geotherm. Res. 56, 1–34.

Bonaccorso, A., 2001. Mt Etna volcano: modeling of ground deformation patterns of recent eruptions and considerations on the associated precursors. J. Volcanol. Geotherm. Res. 109, 99–108.

Bonaccorso, A., Campisi, O., Falzone, G., Puglisi, B., Verladita, R., Villari, L., 1991. Etna Ground deformation: electroptical distance measurements and round tilt, in: Data related to eruptive activity, unrest phenomena and other observations on the Italian active volcanoes-1990. Acta Vulcanol. 1, 265–269.

Bonaccorso, A., Velardita, R., Villari, L., 1994. Ground deformation modeling of geodynamic activity associated with the 1991–1993 Etna eruption. Acta Vulcanol. 4, 87–96.

Bonforte, A., Bonaccorso, A., Guglielmino, F., Palano, M., Puglisi, G., 2008. Feeding system and magma storage beneath Mt. Etna as revealed by recent inflation/deflation cycles. J. Geophys. Res. 113 (B5), 1–13.

Caltabiano, T., Romano, R., Budetta, G., 1994. SO_2 flux measurements at Mount Etna (Sicily). J. Geophys. Res. 99, 12809–12819.

Calvari, S., Coltelli, M., Neri, M., Pompilio, M., Scribano, V., 1994. The 1991–1993 Etna eruption: chronology and lava flow-field evolution. Acta Vulcanol. 4, 1–14.

Clark, A.H., Pearce, T.H., Roeder, P.L., Wolfson, R.I., 1986. Oscillatory zoning and other microstructures in magmatic olivine and augite: Nomarski interference contrast observations on etched polished surfaces. Am. Miner. 71, 734–741.

Coogan, L.A., Hain, A., Stahl, S., Chakraborty, S., 2005. Experimental determination of the diffusion coefficient for calcium in olivine between 900 °C and 1500 °C. Geochim. Cosmochim. Acta 69, 3683–3694.

Corsaro, R.A., Pompilio, M., 2004. Magmatic processes in the shallow plumbing system of Mt.Etna as recorded by compositional variations in volcanics of recent summit activity (1995–1999). J. Volcanol. Geotherm. Res. 137, 55–71.

Costa, F., Chakraborty, S., 2004. Decadal time gaps between mafic intrusion and silicic eruption obtained from chemical zoning patterns in olivine. Earth Planet. Sci. Lett. 227, 517–530.

Costa, F., Dungan, M., 2005. Short time scales of magmatic assimilation from diffusion modeling of multiple elements in olivine. Geology 33, 837–840.

Costa, F., Chakraborty, S., Dohmen, R., 2003. Diffusion coupling between trace and major elements and a model for calculation of magma residence times using plagioclase. Geochim. Cosmochim. Acta 67, 2189–2200.

Costa, F., Dohmen, R., Chakraborty, S., 2008. Time scales of magmatic processes from modeling the zoning patterns of crystals. Rev. Mineralogy Geochem. 69, 545–594.

Costa, F., Coogan, L., Chakraborty, S., 2010. The time scales of magma mixing and mingling involving primitive melts and melt–mush interaction at mid-ocean ridges. Contrib. Miner. Petrol. 159, 173–194.

Dohmen, R., Chakraborty, S., 2007. Fe–Mg diffusion in olivine II: point defect chemistry, change of diffusion mechanisms and a model for calculation of diffusion coefficients in natural olivine. Phys. Chem. Minerals 34, 409–430.

Downes, M.J., 1974. Sector and oscillatory zoning in calcic augites from Mt. Etna Sicily. Contrib. Miner. Petrol. 47, 187–196.

Falsaperla, S., Privitera, E., Spampinato, S., Cardaci, C., 1994. Seismic activity and volcanic tremor related to the December 14, 1991 Mt Etna eruption. Acta Vulcanol. 4, 63–75.

Ghiorso, M.S., Sack, R.O., 1995. Chemical mass transfer in magmatic processes IV. A revised and internally consistent thermodynamic model for the interpolation and extrapolation of liquid–solid equilibria in magmatic systems at elevated temperatures and pressures. Contrib. Miner. Petrol. 119, 197–212.

Giammanco, S., Guerrieri, S., Valenza, M., 1995. Soil CO_2 degassing on Mt Etna (Sicily) during the period 1989–1993: discrimination between climatic and volcanic influences. Bull. Volcanol. 57, 52–60.

Ginibre, C., Kronz, A., Wörner, G., 2002. High-resolution quantitative imaging of plagioclase composition using accumulated backscattered electron image: new constraints on oscillatory zoning. Contrib. Miner. Petrol. 142, 436–448.

Ginibre, C., Wörner, G., Kronz, A., 2007. Crystal zoning as an archive for magma evolution. Elements 3, 261–266.

Helz, R.T., 1987. Diverse olivine types in lavas of the 1959 eruption of Kilauea volcano and their bearing on eruption dynamics. In: Decker, R.W., Wright, T.L., Stauffer, P.H. (Eds.), Volcanism in Hawaii. US. Prof. Paper, 1350, pp. 691–722.

Hibbard, M.J., 1981. The magma mixing origin of mantled feldspars. Contrib. Miner. Petrol. 76, 158–170.

Humphreys, M.C.S., Blundy, J.D., Sparks, R.S.J., 2006. Magma evolution and open-system processes at Shiveluch volcano: insights from phenocryst zoning. J. Petrol. 47, 2303–2334.

Kohn, S.C., Henderson, C.M.B., Mason, R.A., 1989. Element zoning trends in olivine phenocrysts from a supposed primary high-magnesian andesite: an electron- and ion-microprobe study. Contrib. Miner. Petrol. 103, 242–252.

Loucks, R.R., 1996. A precise olivine-augite Mg–Fe-exchange geothermometer. Contrib. Miner. Petrol. 125, 140–150.

Marsh, B.D., 2006. Dynamics of magmatic systems. Elements 2, 287–292.

Metrich, N., Rutherford, M.J., 1998. Low pressure crystallization paths of H2O-saturated basaltic–hawaiitic melts from Mt Etna: implications for open-system degassing of basaltic volcanoes. Geochim. Cosmochim. Acta 62, 1195–1205.

Milch, L., 1905. Über magmatische Resorption und porphyrische Struktur. Neues Jb Miner. Geol. Paläont. 22, 1–32.

Millman-Barris, M.S., Beckett, J.R., Michael, M.B., Hofmann, A.E., Morgan, Z., Crowley, M.R., Vilzeuf, D., Stolper, E., 2008. Zoning of phosphorus in igneous olivine. Contrib. Miner. Petrol. 155, 739–765.

Morgan, D.J., Blake, S., 2006. Magmatic residence times of zoned phenocrysts: introduction and application of the binary element diffusion modeling (BDM) technique. Contrib. Miner. Petrol. 151, 58–70.

Morgan, D.J., Blake, S., Rogers, N.W., DeVivo, B., Rolandi, G., Macdonald, R., Hawkesworth, C.J., 2004. Time scales of crystal residence and magma chamber volume from modeling of diffusion profiles in phenocrysts: Vesuvius 1944. Earth Planet. Sci. Lett. 222, 933–946.

Nakamura, M., 1995. Residence time and crystallization history of nickeliferous olivine phenocrysts from the northern Yatsugatake volcanoes, Central Japan: application of a growth and diffusion model in the system Mg–Fe–Ni. J. Volcanol. Geotherm. Res. 66, 81–100.

Palm III, W.J., 2005. Systems Dynamics2nd Ed. Mcgraw Hill, New York. 834 pp.

Patanè, D., Privitera, E., 2001. Seismicity related to 1989 and 1991–1993 Mt. Etna (Italy) eruptions: kinematic constraints by fault plane solution analysis. J. Volcanol. Geotherm. Res. 109, 77–98.

Patanè, D., Privitera, E., Ferrucci, F., Gresta, S., 1994. Seismic activity leading to the 1991–1993 eruption of Mt Etna and its tectonic implications. Acta Vulcanol. 4, 47–55.

Patanè, D., Di Grazia, G., Cannata, A., Montalto, P., 2008. Shallow magma pathway geometry at Mt Etna volcano. Geochem. Geophys. Geosyst. 9, Q12021. doi:10.1029/2008GC002131.

Pearce, T.H., Kolisnik, A.M., 1990. Observations of plagioclase zoning using interference imaging. Earth Sci. Rev. 29, 9–26.

Petry, C., Chakraborty, S., Palme, H., 2004. Experimental determination of Ni diffusion coefficients and their dependency on temperature, composition, oxygen fugacity and crystallographic orientation. Geochim. Cosmochim. Acta 68, 4179–4188.

Ruprecht, P., Bergantz, G.W., Dufek, J., 2008. Modeling of gas-driven magmatic overturn: tracking of phenocryst dispersal and gathering during magma mixing. Geochem. Geophys. Geosyst. 9, Q07017. doi:10.1029/2008GC002022.

Sato, M., Moore, J.C., 1973. Oxygen and sulfur fugacities of magmatic gases directly measured in active vents of Mt Etna. Philos. Trans. R. Soc. Lond. 274, 137–146.

Scarpa, R., Tilling, R.I., 1996. Monitoring and Mitigation of Volcano Hazards. Springer, Berlin. 841 p.

Singer, B.S., Dungan, M.A., Layne, G.D., 1995. Textures and Sr, Ba, Mg, Fe, K and Ti compositional profiles in volcanic plagioclase: clues to the dynamics of calc-alkaline magma chambers. Am. Miner. 80, 776–798.

Stevens, N.J., Murray, J.B., Wadge, G., 1997. The volume and shape of the 1991–1993 lava flow field at Mount Etna Sicily. Bull. Volcanol. 58, 449–454.

Streck, M., 2008. Mineral textures and zoning as evidence for open system processes. Rev. Min. Geochem. 69, 595–622.

Streck, M.J., Dungan, M.A., Malavassi, E., Reagan, M.K., Bussy, F., 2002. The role of basalt replenishment in the generation of basaltic andesites of the ongoing activity at Arenal volcano, Costa Rica: evidence from clinopyroxene and spinel. Bull. Volcanol. 64, 316–327.

Tonarini, S., Armienti, P., D'Orazio, M., Innocenti, F., Pompilio, M., Petrini, R., 1995. Geochemical and isotopic monitoring of Mt. Etna 1989–1993 eruptive activity: bearing on the shallow feeding system. J. Volcanol. Geotherm. Res. 64, 95–115.

Vance, J.A., 1962. Zoning in igneous plagioclase: normal and oscillatory zoning. Am. J. Sci. 260, 76–760.

Vance, J.A., 1965. Zoning in igneous plagioclase: patchy zoning. J. Geol. 73, 636–651.

Wallace, G.S., Bergantz, G.W., 2002. Wavelet-based correlation (WBC) of zoned crystal populations and magma mixing. Earth Planet. Sci. Lett. 202, 133–145.

Wallace, G.S., Bergantz, G.W., 2004. Constraints on mingling of crystal populations from off-center zoning profiles: a statistical approach. Am. Miner. 89, 64–73.

Wallace, G.S., Bergantz, G.W., 2005. Reconciling heterogeneity in crystal zoning data: an application of shared characteristic diagrams at Chaos Crags, Lassen Volcanic Center California. Contrib. Miner. Petrol. 149, 98–112.

Zellmer, G.F., Blake, S., Vance, D., Hakesworth, C., Turner, S., 1999. Plagioclase residence times at two island arc volcanoes (Kameni islands, Santorini and Soufriere, St. Vincent) determined by Sr diffusion systematics. Contrib. Miner. Petrol. 136, 345–357.